Secondary fluorescence in WDS: the role of spectrometer positioning

Ben Buse, Jon Wade, Xavier Llovet, Stuart Kearns, and John J Donovan

Abstract

Secondary fluorescence, typically a minor error in routine electron probe microanalysis (EPMA), may not be negligible when performing high precision trace element analyses in multiphase samples. Other factors, notably wavelength dispersive spectrometer defocusing, may introduce analytical artefacts.

To explore these issues, we measured EPMA transects across two material couples chosen for their high fluorescence yield. We measured transects away from the fluorescent phase, and at various orientations with respect to the spectrometer focal line. Compared to calculations using both the Monte Carlo simulation code PENEPMA and the semi-analytical model FANAL, both codes estimate the magnitude of SF, but accurate correction requires knowledge of the position of the spectrometer with respect to the couple interface. Positioned over the fluorescent phase or otherwise here results in a factor of 1.2-1.8 of apparent change in SF yield.

SF and spectrometer defocusing may introduce systematic errors into trace element analyses, both may be adequately accounted for by modelling. Of the two, however, SF is the dominant error, resulting in 0.1 wt% Zn apparently present in Al at 100 μm away from the Zn boundary in an Al/Zn couple. Of this, around 200 ppm Zn can be attributed to spectrometer defocusing.

Introduction

Secondary fluorescence (SF), where characteristic x-rays are excited by either continuum- or characteristic x-rays possessing energies above their critical excitation edge, may arise at significant distances from the electron beam point of impact. This can be significant when measuring trace elements in multiphase samples, where the SF contribution arises from adjacent phases containing the element of interest in high concentration (e.g. Adams and Bishop (1986)). Examples include diffusion profile measurements, redox sensors and geo-thermometers (e.g. Ti in quartz). In such cases, it is necessary to subtract the SF contribution to obtain the correct concentration in the phase being analysed; this can be done either by preparing material couples and measuring SF contribution (Adams and Bishop (1986)) or by calculating SF (e.g. Myklebust & Newbury 1995). For high-precision trace element analysis, the positioning of the spectrometer must be considered, to accurately correct for SF (Fournelle et al, 2005; Llovet & Salvat, 2017). This determines the material path – that is, the path through the material by which the fluoresced x-rays travel to the detector - which in turn determines the degree of x-ray absorption (Llovet et al. 2012). Spectrometer placement with respect to the sample also determines the extent to which the source of fluorescent x-rays is in focus with respect to the spectrometer, a factor that is often overlooked. Although the spectrometer is focused on the point of analysis, SF x-rays originate from a range of distances from it (as large as hundreds of microns) and are displaced relative to the focal position.

Electron probe microanalysis (EPMA) relies on Rowland circle wavelength dispersive spectrometers (WDS), which utilise a type of Bragg spectrometer where the incident x-rays are reflected into a proportional counter using a crystal. WDS crystals are curved to twice the radius of the Rowland circle upon which the sample, crystal and counter all lie. Typical Rowland circles for commercially available spectrometers range from 100 mm (H-type) and 140 mm for JEOL microprobes, 160 mm for CAMECA microprobes and 210 mm for Oxford Instruments spectrometers. On a JEOL microprobe

the suffix H e.g. PETH denotes a PET crystal on a H-type spectrometer, whilst the suffix L e.g. PETL denotes a large PET crystal on a regular 140 mm Rowland circle.

Two variants of reflecting crystals are employed; a Johann and a Johannson type crystal, the latter in addition to being curved is ground to the radius of the Rowland circle. In both cases the curvature of the reflecting crystals maximises the solid angle of the incident x-rays. SF arises when x-rays are excited in a neighbouring phase by x-rays possessing energies above the critical excitation energy of the fluoresced x-rays. These SF x-rays may therefore be excited a significant distance from the point of analysis and, given the spectrometers finite focal area, may be collected in addition to those originating from the analytical point.

Spectrometer defocusing is most readily observed when a beam scan x-ray map (using a rastered beam) is acquired over a large area; the spectrometer is in focus along a line perpendicular to the plane of the Rowland circle (Figure 1a), but counts diminish away from the centre of the focal line (e.g. Newbury et al. 1988). This defocusing arises when the x-ray source, crystal and detector no longer lie on the Rowland circle and the spectrometer deviates from the geometry required to satisfy the Bragg equation. As the source becomes displaced, spectrometer defocusing is at a maximum in the plane of the Rowland circle (displacement in x on Fig 1a) and diminishes to zero perpendicular to the plane of the Rowland circle (displacement in y on fig 1a). The amount of defocusing resulting from the displacement of the source in x, expressed in terms of the change in sin(θ) angle reflected, is given by the equation:

$$\sin(\Delta\theta) = \Delta x \sin(\psi) / 2R \sin\theta \qquad (1)$$

where $2R \sin\theta$ is the distance between the x-ray source and reflecting crystal, Δx is the amount of lateral source displacement, ψ is the take-off angle (40^o) and R is the radius of the Rowland circle (Marinenko et al. 1988). Hence, spectrometer defocusing can be reduced by increasing the distance between the x-ray source and reflecting crystal; for example, for elements which may be analysed on several crystals, using the reflecting crystal with the smaller d-spacing, Ti on LIF for 140 mm Rowland circle $2R \sin\theta$ = 191 mm compared to 87.9mm on PET. The impact of defocusing on x-ray intensities will vary with spectral resolution. Although only vertical spectrometers are considered in this study, inclined spectrometers exhibit poorer lateral resolution due to the focal plane being inclined relative to the vertical. Therefore, any influence arising from spectrometer defocusing will be greater for spectrometers orientated away from the vertical.

The influence of spectrometer defocusing on measured SF contributions was first suggested by Adams and Bishop (1986) to explain discrepancies in measured and calculated SF contributions, and subsequent work (e.g. Dalton and Lane 1996, Llovet & Galan 2003) attempted to measure SF along the "focus line of the spectrometer" (Dalton & Lane 1996). If spectrometer defocusing is not considered, any SF correction made by assuming the shortest linear distance from point of analysis to the fluorescent phases may result in an over-correction, and hence the concentration in the sample will be under-estimated.

To assess the importance of spectrometer orientation on trace element analyses in multiphase samples, we measure the SF contribution at various orientations with respect to the detector focal line and with different material paths to the detector. The aim is to evaluate the various errors associated with spectrometer positioning. We show that a low magnification beam scan map may be used to obtain a good agreement between measured and modelled SF contributions. Moderate corrections are required when the spectrometer is defocussed – that is, when the fluorescent phase does not lie along the spectrometer's line of focus. This approach of correction for both SF as a function of spectrometer position with respect to the fluorescing phase boundary, and the potential

for spectrometer defocusing, allows for a correct subtraction of SF and hence accurate trace element analyses in multiphase samples.

Materials and methods

To quantify the effect of spectrometer defocusing, an aluminium and zinc metal material couple was made using spectroscopically pure metals. These were chosen for the significant Zn SF that arises when measuring Al metal at large distances from the interface, especially when using high accelerating voltages. The two metals were pressed together and set in epoxy resin resulting in a good contact such that there was no physical gap apparent along the join. A second couple made of molybdenum and titanium was prepared in a similar fashion. The SF contribution of Zn Kα arising from SF was measured along transects through the Al, with the spectrometers aligned on the Al side of the couple (here referred to as the Al-path). All the transects were measured perpendicular to the material interface with Zn. The orientation of the sample with respect to the focal line of the detector, given by angle α, was varied (see figure 1b), with transects measured at α = 0° - i.e. with the material boundary lying perpendicular to the focal plane - and at α angles in the range 10-90° (see Figure 1). In the case of the transect measured at α = 0°, the x-rays pass along the interface to the detector through both components of the couple, requiring further considerations when modelling. Transects made at α angles in the range 10-90° avoid this complication since the resultant x-rays pass solely through one half of the material couple. In addition, secondary fluoresced Zn x-rays were also measured with the spectrometers aligned on the Zn side of the couple (the Zn-path). By measuring the effect of the spectrometer placement with respect to the material boundary, we can assess the effect that the material path – here either Al or Zn – has on the measured SF yield. To remove any possibility of extraneous fluoresced x-rays arising from the sample holder, we used an aluminium sample holder - measurement of a zinc-free aluminium standard confirmed the absence of other Zn contributions. Measurements were made on a JEOL 8530F electron microprobe, at the University of Bristol, using a LIFH crystal. Analytical conditions were chosen to maximise the SF signal, with an accelerating voltage of 30 kV, a beam current of 500 nA, and a spot size of 1 µm. Count times were 60 seconds on peak and 60 seconds on background. Zn was measured whilst the Al content was specified.

To explore the effects of SF arising from softer x-rays excited when analysing a denser material, we used a similar approach with a Ti-Mo couple, with the SF contribution of Ti Kα measured along several transects through the Mo. In this example, the transects were oriented at α = 11.5° and α = 101.5°. The specific orientation of these transects was motivated by the azimuthal position of the spectrometer around the electron optics system (-11.5° with respect to the horizontal X-axis). These orientations mean the SF x-rays were only absorbed in the Ti side of the couple, which allows direct comparison with the geometries assumed by the FANAL calculations (see below). The measurements were made on a JEOL 8230 electron microprobe using a PETL crystal, at the University of Barcelona. Analytical conditions were an accelerating voltage of 25 kV, a beam current of 500 nA, and a nominal spot size of 1 µm. Again, count times were 60 seconds on peak and 60 seconds on background.

Since the SF arises from a neighbouring phase, there is no appropriate matrix correction. For clarity, we therefore report k-ratios as apparent wt. % or apparent ppm.

Modelling secondary fluorescence

We calculated the SF contribution using the Monte Carlo simulation programme PENEPMA (Llovet and Salvat, 2017). Two detectors were simulated, both of 180° azimuthal aperture collecting x-rays between 35-45° take-off angle, positioned either side of the material couple boundary. The large

semi-circular detectors both reduce simulation time and increase precision. This geometry allows direct comparison with FANAL calculations, which presume the detector is positioned only over the side of the fluorescing material. The simulations achieved a 1% relative error (at 3 sigma level) on both the standard intensity and the unknown intensity at short distances from the interface (≤ 75 μm), rising to 4% at 450 μm. For the special case of a transect oriented parallel to the focal line of the detector, where x-rays pass through two materials on route to the detector, the effect of the azimuthal width $(\Delta\phi)$ of the detector aperture on modelled results was investigated. Simulations were made at 100 μm with a detector aligned to the material interface and the azimuthal width was varied.

FANAL provides an easy and fast calculation of SF (Llovet et al. 2012; Donovan et al 2012) but, unlike PENEPMA, implements only a semi-analytical model for the calculation of SF near a planar, perpendicular material boundary. FANAL obtains the intensities of primary photons for both materials used in the couple and the standard, using a version of PENEPMA optimized for this task (see Llovet et al 2012). Importantly, the approach taken in the FANAL code makes two assumptions – firstly that that the detector is located only over the fluorescing phase, and secondly that the emission of bremsstrahlung photons is isotropic. The first assumption means that only x-ray absorption through the fluorescent phase needs to be considered, whilst the second greatly simplifies the analytical model upon which FANAL is based.

To correct for secondary fluorescence the modelled SF k-ratios are subtracted from the experimental k-ratios, which should be first corrected for spectrometer defocusing.

Correction for spectrometer defocusing

To adequately account for the influence of SF on trace element analysis, it may be necessary to calibrate the analytical spectrometer's rate of defocusing with respect to distance from the focal line. This was achieved by acquiring x-ray maps, with the beam rastered over a large area (fig 2), on Zn and Ti metal standards. This allows the reduction in x-ray intensity as a result of spectrometer defocusing to be calculated as follows. Firstly, x-ray counts were extracted from a line (X-Y; Figure 2 a & b) possessing the same orientation as the transect. For example, Figure 2 shows the measurements of the material couple where the Zn interface (source of Zn X-rays) was to the top left with respect to the electron beam point of impact (position of spectrometer focus). Secondly, the ratio of maximum intensity to measured intensity was calculated and described using a polynomial function (the polynomial required varied between 2nd to 6th order to achieve a data fit of approximately ± 2% relative). To correct for defocusing, the measured data was then multiplied by the polynomial function, with x being the distance to the interface. Note that we implicitly assume that SF is emitted from a single point located on the interface of the two materials.

Results

Zn-Al couple

Transects where x-rays pass through a single material to detector

Figure 3 shows the results for both PENEPMA and FANAL simulations for a transect in Al away from the Zn interface. Zn Kα k-ratios are greater where the material path to the detector is aluminium (Al-path) by a factor of 1.2 increasing to 1.8 with distance. The difference between the paths is due to the lower x-ray absorption of Zn in Al (Llovet et al. 2012). In general, the two codes show a good agreement although the assumptions made in the FANAL model mean that it can only be compared to PENEPMA where Zn is the material path to the detector (Zn-path) – i.e. where the simulated PENEPMA detector is located over the Zn (fluorescent) component of the couple. The slight deviations between the two models likely relate to the treatment of the bremsstrahlung emission

which FANAL assumes to be emitted isotropically, whilst PENEPMA uses an intrinsic theoretical angular distribution (Acosta et al. 2002, Llovet et al. 2011). Here the simplification used by the FANAL model becomes important since all the SF results from bremsstrahlung emission rather than primary x-ray emission.

Experimental results for the Zn-Al couple are shown in Figure 4. The measured zinc k-ratio decreases with distance from the interface as the influence of SF decreases. Fig 4a shows the situation assumed by FANAL (see Figure 3), where the spectrometer is located over the fluorescing phase (here the Zn-path), while (4b) shows the results for the Al-path. At distances < 100μm, assuming the correct sample geometry is used, that is, the correct material path to the detector is simulated, the measurements show a reasonable approximation to the modelled data. The measured intensities for the Al-path are, however, higher than the Zn-path due to lower x-ray absorption. At distances > 100 μm the measured intensities are lower than predicted by PENEPMA which is consistent with spectrometer defocusing.

To show the magnitude of defocusing effects, the residual concentration, that is, the amount of measured Zn that remains apparent in the sample after SF contributions are accounted for, is shown in figure 5. This shows the residual when SF alone and SF plus a defocusing correction is subtracted from the measured concentrations. All the Zn is derived from SF and therefore the residual should be zero. Simply correcting for SF results in a small negative residual (hundreds of ppm), which is a small percentage of SF contributions (thousands of ppm) at short distances, but this becomes increasingly significant at longer distances as the SF contributions are reduced. Adjusting the measured data for defocusing effects decreases the residual over distances 50-200 μm over which defocusing is significant. At distances > 200μm correcting for defocusing is problematic, and results in a significant over correction. Additionally, at these distances defocusing is severe, but the measured SF contribution does not decrease as one may expected. The reasons are unclear and may reflect fluorescence of the Zn material from chamber scattered x-rays.

Transects where x-rays pass through two materials to detector

Here the instrument detector is aligned along the material interface. Simulations using a similar geometry show the modelled results are strongly dependent on the detector aperture width (figure 6), and a realistic aperture width is required. On a JEOL EPMA, the distance of the analytical source from the reflecting crystal, in this case a LIFH crystal reflecting Zn Kα radiation, is 71 mm. The reflecting crystal position corresponds to the detector in the simulation, and a typical crystal is approximately 1.7 cm wide resulting in a 10° azimuthal aperture being a reasonable approximation for the purposes of the simulation. Due to the small solid angle of the simulated detector, simulations were only made for a single point along the transect in Al, 100 μm from the interface. Using this simulation, the more computationally efficient 180° azimuthal aperture may be used to correct the Zn-path modelled results, by applying a scaling factor (the difference in k-ratio between the Al-Zn path with a 10^{o} azimuthal aperture and the Zn path with a 180^{o} azimuthal aperture, at 100 μm).

Figure 7 compares the experimental and modelled results. The experimental results show a reasonable agreement with the simulation data for a 10° azimuthal aperture, which approximates the effective width of a real detector. If this is neglected a substantial error results if the Al path to detector is used.

Ti-Mo couple

In the case of the measure Ti Kα k-ratio, there is a satisfactory agreement between the predictions of FANAL and PENEPMA (Figure 8). In a high-Z element, such as Mo, electron trajectories are more rapidly randomized by elastic scattering than in a low-Z material, such as Al. The angular distribution of continuum photons is therefore less sensitive to their intrinsic angular distribution. The higher density material present in the couple – in this case Mo - significantly increases the absorption of bremsstrahlung x-rays, resulting in greater attenuation and hence a lower SF contribution with distance increases from the boundary. This results in lessening of the influence of SF with distance – for the Al-Zn couple, Zn SF was measured at 200 ppm at a distance of 300μm, whilst Ti reaches 200 ppm at only 40μm from the boundary. This rapid attenuation of fluoresced x-rays results in minimal defocusing observed at $\alpha = 101.5°$ and within the analytical error. The small magnitude of the defocusing effect compared to the SF contribution, over these distances, is clearly seen in the comparison of the two curves in (fig 8b). The position of the detector with respect to the interface results a change in concentration of a factor of 1.25. This is a larger error than that generated by spectrometer defocusing close to the interface, but the error associated with defocusing increases to comparable magnitude at the long distances.

Again, the correction for spectrometer defocusing proposed here assumes that SF is emitted from a single point, located precisely on the interface. PENEPMA simulations show that Ti Kα x-rays emitted from a Ti-Mo couple do not arise from a point source; when the beam impacts at 25 μm from the boundary, the maximum region over which the Ti Kα x-rays are actually generated extends up to ~150 μm either way along the boundary direction and ~ 100 μm into the Ti (Figure 9). However, the maximum intensity is localized close to the boundary, with 75% of the excited x-rays generated within 40 μm either way along the boundary and 40 μm into the Ti, and rapidly decreases in both directions. Given the complexities and material specific nature of the excitation volume, and the limited volume over which the majority of SF x-rays are generated, a point source was assumed to be a valid assumption for the purpose of correcting spectrometer defocusing.

To calculate the error associated with using this assumption, the results were compared to a more accurate 2D defocusing correction using simulated x-ray emission maps (see Fig 9) as follows: for selected distances to the boundary (10, 25, 50 and 100 μm), the simulated x-ray emission maps were multiplied pixel by pixel by the defocusing map and the resulting maps were integrated so as to yield the corrected x-ray intensities at the specific distance.
These intensities were then compared with those obtained by using one single pixel for the correction (the first pixel situated along the transect within the fluorescing phase). The difference between assuming an x-ray emission region and an x-ray emission point for the defocusing correction was found to be less than 5%. Nevertheless, the difference between the experimental data and the calculated data (corrected for defocusing effects assuming a point x-ray source) appears to be larger than 5%. The reason for this disagreement is not fully understood, and it would obviously be interesting to make similar measurements and calculations in other systems.

Discussion

The ability to rapidly estimate the SF contribution arising from neighbouring phases and correct for their influence on minor and trace element analyses, has proven valuable, especially where high spatial resolution analysis (Wade and Wood, 2012) or element diffusion profiles are desired. On the other hand, the orientation of the spectrometer with respect to neighbouring, fluorescent phases has been largely overlooked, even though its effect may not be negligible if high accuracy analyses are required. Although simulation codes are capable of adequately correcting for SF in real analyses,

they do require knowledge of both sample and spectrometer geometries such that they do not over- or under compensate. The correction process, detailed above, allows the SF contributions for varying spectrometer orientations to be calculated, which may then be subtracted from measurements to give the primary x-ray intensity. This requires knowledge of the transect orientation with respect to the spectrometer's focal line and a beam scan map of the spectrometer from which the intensity loss with source displacement can be calculated. In the case that several spectrometers are used to improve counting statistics (see e.g. Wark and Watson, 2006), the proposed correction should be applied to the x-ray intensities measured by each spectrometer, before obtaining the sum of all intensities. To minimise instrument time, a beam scan map could be calculated from a WD peak scan using the method of Myklebust et al. (1986), since the effect of scanning the beam (deflecting the source) in the plane of the Rowland circle is equivalent to shifting the crystal angle (Myklebust et al. 1986, Swyt & Fiori 1986).

In most scenarios, spectrometer defocusing represents, at worst, only a minor correction to trace element analyses compared to the influence of SF, and is most likely lost within the analytical uncertainty. For instance, in the example of the Al-Zn couple here, not compensating for defocusing results in a relative error of 6% or 140 ppm Zn, compared to that generated by SF of 2160 ppm at 50 μm from the interface. The errors, however, rapidly increase at long distances where defocusing is 20% and 60% of that generated by SF at 100 μm and 200 μm respectively. The approach used here with a simple material couple, with a planar, vertical boundary, is well suited to modelling and correction using FANAL, provided the fluorescing material forms the path to the detector. Many real-world samples however, require more robust simulation using PENEPMA which allows for greater flexibility in sample geometries, although it should be noted that for large distances from the boundary the effect of geometry will be small. The results for a planar couple however, provide insight on the circumstances for which a correction for defocusing would be most beneficial and occurs at relatively long distances (> 50-100 μm) to the material boundary. At very long distances (≥ 300 μm), corrections arising from spectrometer defocusing may be very large (700%-1400%). Importantly, the results suggest a tendency to overcorrect at these long boundary distances. Under these circumstances counting errors are magnified and measurement is unadvisable, with reorientation of the sample to avoid defocusing being preferable whenever possible.

The need to account for spectrometer defocusing therefore only arises where the effect on SF contribution arising from spectrometer orientation constitutes a significant part of the error budget. This is most problematic where the material analysed is low density, has minimal attenuation of the fluorescing x-ray, and the resultant SF x-ray has a relatively high fluorescence yield, such as in the Al-Zn couple used here.

The placement of the detector with respect to the fluoresced side of the interface results in a significant error - in the case of the Al-Zn couple, the relative difference between a spectrometer placed on one side or other of the boundary results in a factor of 1.2-1.8 change in SF yield. Additionally, the error increases with distance from the interface, but its magnitude and variation with distance depends on the difference in absorption between the two materials, and is greatest where there is a significant difference in density or mass attenuation coefficient. In the case of Ti-Mo the spectrometer placement resulted in an error of 1.25 which varied little with distance. Measuring Ti in quartz, an often used geo-thermometer, provides a good example of where accounting for spectrometer orientation is important. SF of Ti in quartz is observed at long distances away from adjacent materials (e.g. rutile); Wark and Watson (2006) measured 100 ppm in quartz at 100 μm away from rutile (using a quartz-rutile material couple). At this distance, for maximum spectrometer defocusing, measured SF contributions would be reduced by about 30 % using a PET crystal. In

addition to spectrometer orientation, switching from PET to LIF would reduce defocusing by increasing the source to crystal distance at which Ti Kα is measured but at the expense of x-ray intensity.

Spectrometer orientation is less important for SF of Ca in olivine. Dalton and Lane (1996) showed that Ca is fluoresced at significant concentrations up to ca. 40-80 μm from interfaces with phases containing Ca. This equates to intensity reductions for maximum spectrometer defocusing of 15-25%. The requirement for correcting for spectrometer orientation will therefore depend on the degree of defocusing (the orientation of the interface with respect to the detector) and the analytical error (see Dalton & Lane 1996, Llovet et al. 2012).

Conclusions

The SF contribution may result in substantial errors when measuring trace elements at high precision in multiphase samples. The ability to accurately calculate the SF contribution to allow for its subtraction and give actual elemental concentrations depends significantly on spectrometer orientation. Spectrometer orientation is important in determining the material through which x-rays pass through to the detector, and this results in a substantial variation in the SF contribution, both observed and simulated. Spectrometer orientation may result in a reduction of the measured SF where the source of SF x-rays is defocused with respect to the spectrometer. This effect is small compared to the SF contribution, although at long distances its contribution can change the apparent SF by tens of percent relative. Defocusing effects on SF are at a maximum when interfaces are perpendicular to the plane of the Rowland circle (parallel to the spectrometer line of focus). Ignoring these effects leads to a small but systematic error in our ability to correct SF contribution and subtract it from measurements to give primary x-ray intensities.

At short distances, errors from spectrometer defocusing are not significant given the other errors involved in calculating the SF contribution. However, where the reduction in intensity from spectrometer defocusing exceeds errors associated with the SF calculation, it should be considered.

In the example of Ti-Mo, SF decreases rapidly from the interface and error arising from defocusing is within analytical error. In contrast, the example of Zn fluoresced from an Al-Zn couple, SF extends a significant distance from the interface and defocusing results in a significant error. The error is in excess of 20% of the SF contribution at distances > 100μm, and exceeds the analytical error of 3% relative (at 3 sigma level) at 100μm. Defocusing errors may be addressed by either:

(a) reducing defocusing by selecting a reflecting crystal with a smaller d-spacing. This is however accompanied by a loss of x-ray intensity.
(b) correcting the measured intensities for spectrometer defocusing prior to correcting for SF.

Transects at small angles to the focal line of the detector are obviously preferable. However, in the case of transects made parallel to the focal line, with x-rays passing along the interface to the detector, the aperture of the instrument detector must also be considered and used to scale the simulated results.

The results presented here suggest spectrometer defocusing has a large effect on measured SF intensities at distances > 50-100 μm from the source of x-rays. This is, however, dependent both on the width of the x-ray peak and spectrometer resolution.

The examples given demonstrate the importance of correcting SF by simulating realistic geometries which correspond to the sample geometry and the instrument configuration; critically the position of the detector with respect to the material interface must be replicated. The current FANAL code works well when the instrument detector is on the fluorescent side of the boundary and x-rays pass through a single material to the detector, giving fast accurate results for this situation. However, care must be taken when relating this to real-world analyses of SF arising from a planar, or non-symmetrical, boundary. In these cases, incorrect assumptions regarding the geometry of the boundary and spectrometer when using simulations to remove these effects, may result in relative errors in excess of 100%. The more detailed approach allowed by PENEPMA allows accurate calculation of SF for all geometries but does require the appropriate geometry to be configured in the input files.

Acknowledgements

We would like to thank Charles Clapham (University of Bristol) for his assistance in making the Al-Zn material couple and Erkki Heikinheimo (Aalto University) for preparing the Ti-Mo couple. We would like to thank the reviewers for their detailed comments.

References

Acosta, E., Llovet, X., & Salvat, F. (2002). Monte Carlo simulation of bremsstrahlung emission by electrons. *Appl Phys Lett* **80**, 3228–3330.

Adams, G. E. & Bishop, F. C. (1986). The olivine-clinopyroxene geobarometer: experimental results in the CaO-FeO-MgO-SiO, system. *Contrib Mineral Petrol* **94**, 230-237

Bragg, W.H. & Bragg, W.L. (1913). The reflection of X-rays by crystals. *Proc R Soc Lond A Math Phys Sci* **88**, 428-438

Dalton, J.A. & Lane, S.J. (1996). Electron microprobe analysis of Ca in olivine close to grain boundaries: The problem of secondary X-ray fluorescence. *Am Mineral* **81**, 194-201

Donovan, J., Llovet, X., & Salvat, F. (2012). High Speed Matrix and secondary fluorescence effects from fundamental parameter Monte Carlo calculations. *Microsc Microanal* **18,** 1742-1743

Fournelle, J., Kim, S., Perepezko, J.H. (2005) Monte Carlo simulation of Nb Ka secondary fluorescence in EPMA: comparison of PENELOPE simulation with experimental results, *Surf. Interface Anal* **37**, 1012-1016

Kluckner, M., Brandl, O., Weinbruch, S., Stadermann, F.J., Ortner, H.M. (1997) A Method to Correct Defocused Element Distribution Maps in Electron Probe Microanalysis, *Mikrochim. Acta* **125**, 229-234

Llovet, X. & Galan, G. (2003). Correction of secondary X-ray fluorescence near grain boundaries in electron microprobe analysis: Application to thermobarometry of spinel lherzolites. *Am Mineral* **88** 121-130

Llovet, X., Pinard, P.T., Donovan, J.J. & Salvat, F. (2012). Secondary fluorescence in electron probe microanalysis of material couples. *J Phys D: Appl Phys* **45** 225301 (12pp)

Llovet, X., & Salvat, F. (2017). PENEPMA: A Monte Carlo Program for the Simulation of X-Ray Emission in Electron Probe Microanalysis. *Microsc. Microanal.* **23**, 634–646, 2017

Marinenko, R.B., Myklebust, R.L., Bright, D.S. & Newbury, D.E. (1989). Defocus modelling correction for wavelength dispersive digital compositional mapping with the electron microprobe. *J Microsc* **155,** 183-198

Myklebust, R.L., Newbury, D.E., Marinenko, R.B. & Bright, D.S. (1986). Defocus modeling for compositional mapping with wavelength dispersive x-ray spectrometry. In Microbeam Analysis-1986, Romig Jr., A.D. & Chambers, W.F. (Eds.) pp. 495-497. San Francisco : San Francisco Press.

Myklebust, R.L. & Newbury, D.E. (1995). Monte carlo modelling of secondary x-ray fluorescence across phase boundaries in electron probe microanalysis. *Scanning* **17**, 235-242

Newbury, D.E., Marinenko, R.B., Bright, D.S. & Myklebust, R.L. (1988). Computer-aided imaging: Quantitative compositional mapping with the electron probe microanalyzer. *Scanning* **10** 213-225

Swyt, C.R. & Fiori, C.E. (1986). Large-field x-ray compositional mapping with multiple dynamically focussed wavelength-dispersive spectrometers. In Microbeam Analysis-1986, Romig Jr., A.D. & Chambers, W.F. (Eds.) pp 482-484. San Francisco: San Francisco Press

Wade, J. & Wood, B. J. (2012). Metal-silicate partitioning experiments in the diamond anvil cell: A comment on potential analytical errors. *Phys Earth Planet Inter* **192-193**, 54-58

Wark, D.A. & Watson, E.B. (2006). The TitaniQ: A Titanium-in-quartz geothermometer. *Contrib Mineral Petrol* **152,** 743–754

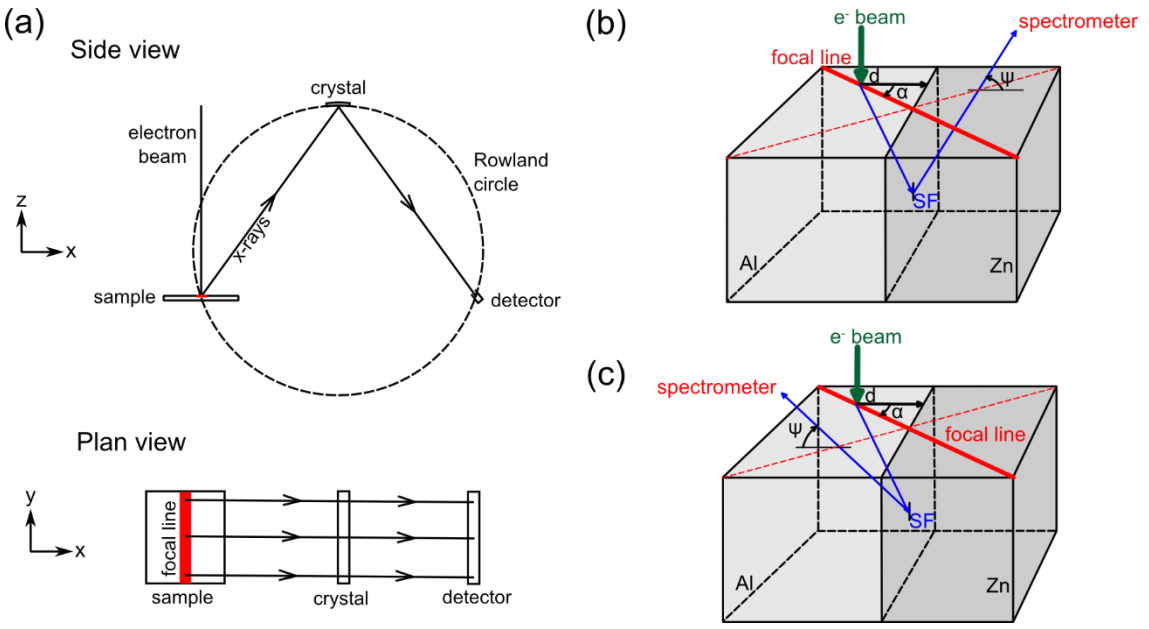

Figure 1. (a) Schematics showing the orientation of the spectrometer focal line with respect to the Rowland circle. (b & c) Schematic diagrams showing the emission of SF from an Al-Zn couple when the electron beam impinges on the Al phase, at a distance d from the interface. The measuring spectrometer is located on the Zn phase for (b) and on the Al phase for (c). The SF transect is measured along a line perpendicular to the interface and oriented at an angle α with respect to the focal line of the spectrometer. α is changed by rotating the sample. Ψ is the take-off angle.

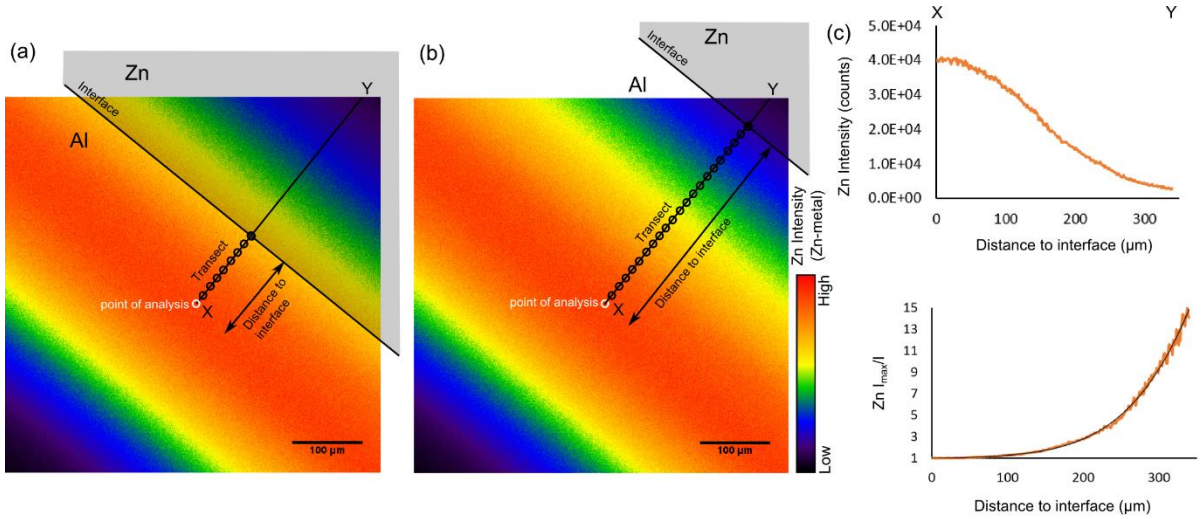

Figure 2. To correct transects for defocusing, a beam scan map is used - this records spectrometer defocusing as the source is displaced away from the focal line. (a, b) Experimental configuration of the transect orientated at 90° to focal line, overlain on the beam scan map acquired on a Zn metal standard. This approach allows the extraction of a line profile from the beam map shown in fig 4c. As the distance to the interface is increased, the spectrometer defocusing becomes pronounced – this is illustrated by the drop in Zn intensity from (4a) to (4b). (c) Extracted intensity for the line profile shown in fig 4a (4c top). The ratio of maximum x-ray intensity to intensity along the line profile, Imax/I (4c lower), is used to correct the transect measurements by fitting a polynomial function.

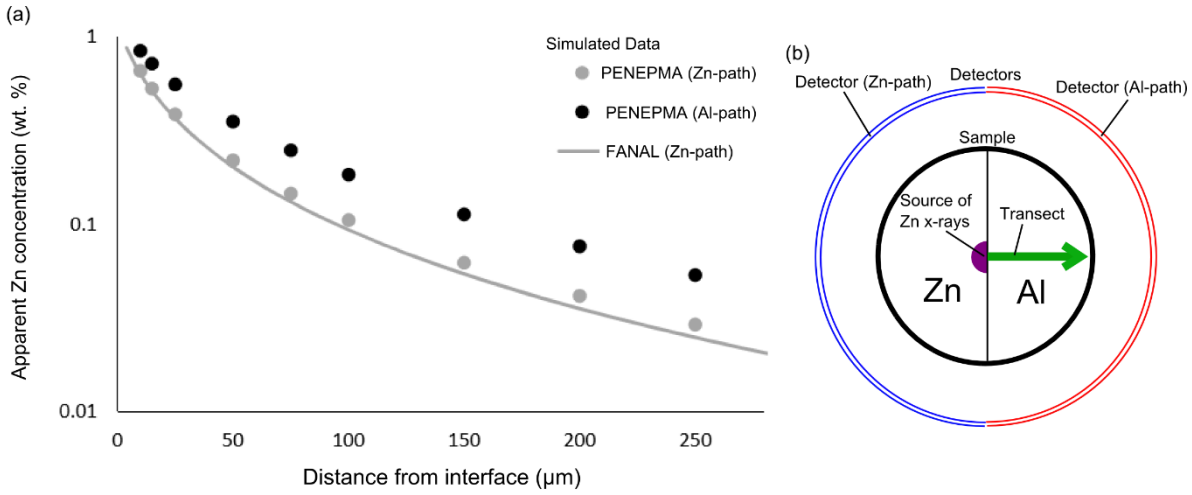

Figure 3a. Calculated contributions from Zn secondary fluorescence arising from analysis of Al in a Zn-Al couple. Depending on the position of the detector, the fluorescent Zn x-rays pass through either Zn or Al (2b). Calculations are made using both PENEPMA and FANAL; FANAL assumes that x-rays pass through the material being fluoresced (here Zn).

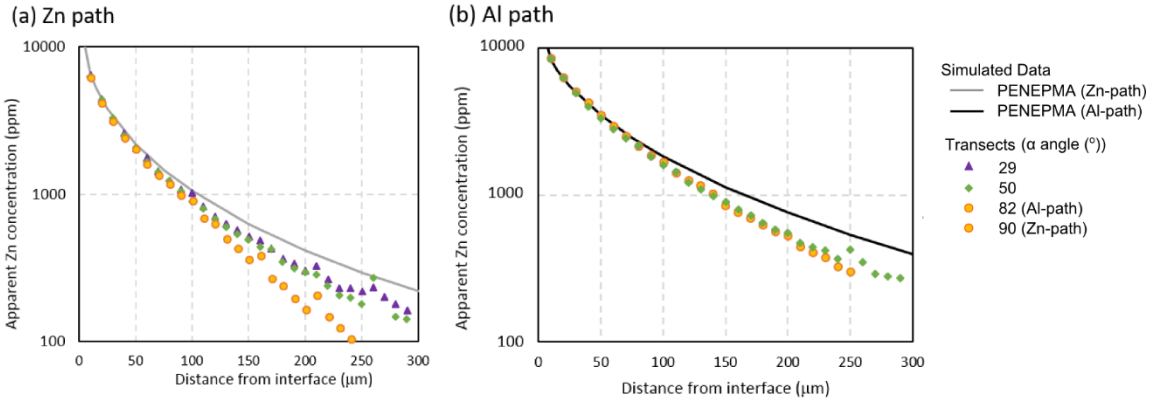

Figure 4. Measured SF contributions of Zn Ka in Al for different sample orientations and paths to the detector: (a) Zn path to detector, (b) Al path to detector. To illustrate the error when using the wrong detector position, the concentration calculated from a detector on the opposite side of the material interface is shown. Symbol size approximates analytical errors (3σ).

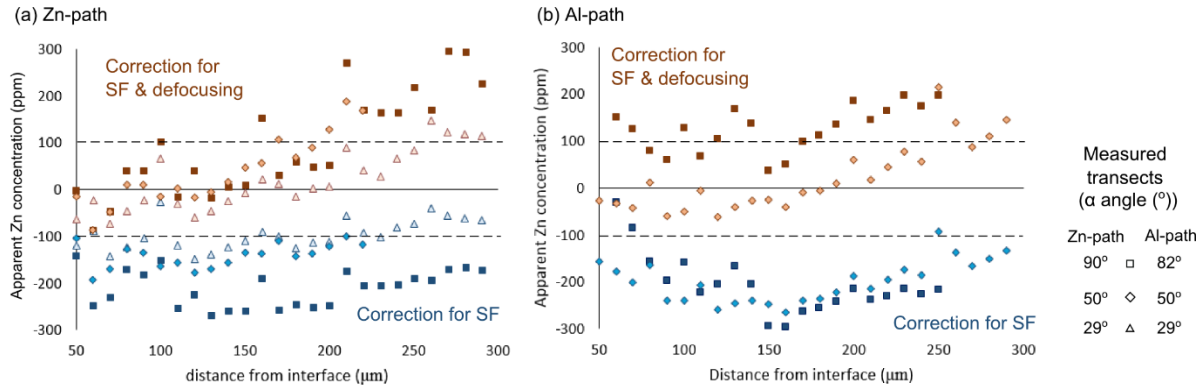

Figure 5. Correcting the measured transects which suffer defocusing for SF (blue colours) and SF plus defocusing (red-orange colours). All the Zn Ka originates from SF and therefore the corrected data should equal zero. To illustrate the improvement made by correcting the data for defocusing, a zone +/- 100 ppm is marked on the graphs by dashed lines.

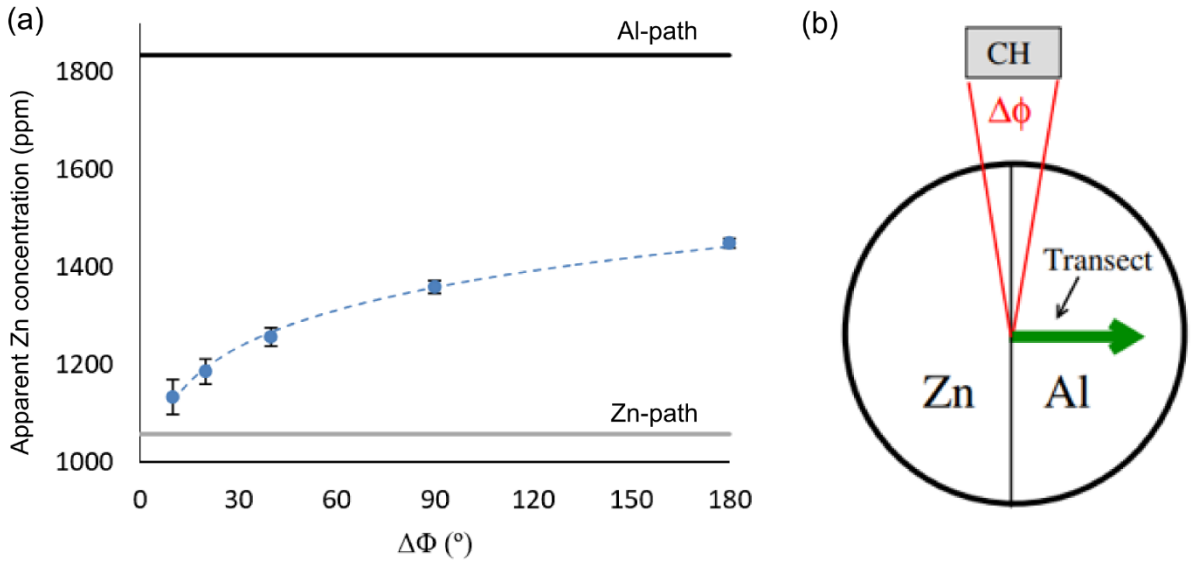

Figure 6 Simulated secondary fluorescence contributions (3a) when the transect is parallel to the focal line of the detector, with x-rays passing along material interface to the detector (3b) as a function of detector azimuthal aperture. Simulations were made for a point along the transect in Al, at a distance of 100 µm from the interface.

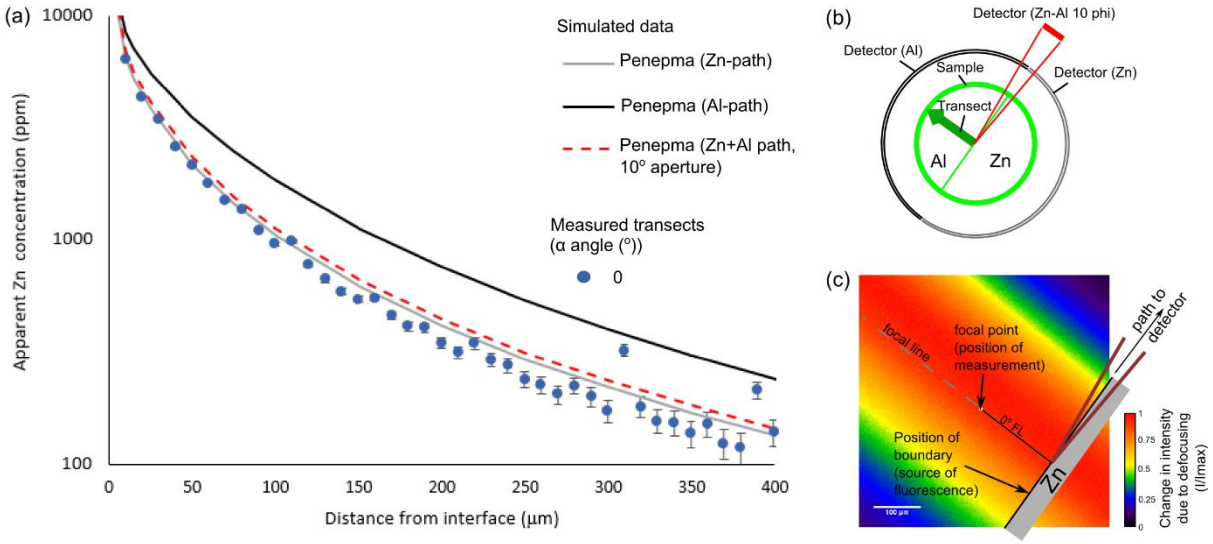

Figure 7. Comparison of the measurements to the simulated data for different detector configurations, including a realistic simulation where the detector is aligned along the interface with a 10° azimuthal aperture. Using a realistic detector width minimises the mismatch between simulation (red line) and the measured data (blue dots). (b) Schematic showing the geometries of the simulated detectors, and (c) schematic showing the geometry of the sample and instrument detector, where the geometry is overlain on a map of spectrometer defocusing.

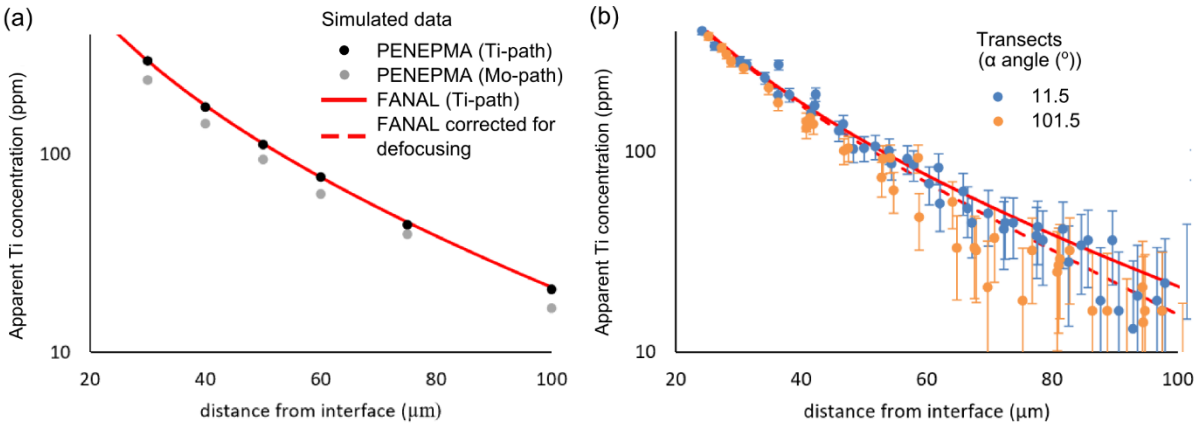

Figure 8. (a) Comparison of measured, calculated (FANAL) and simulated (PENEPMA) Ti k-ratios versus beam distance to boundary for a transect in-focus in a Ti-Mo couple. (b) Comparison of measured, calculated (FANAL) and calculated -and corrected for defocusing effects- (FANAL corrected) Ti k-ratios for a transect out-of-focus in a Ti-Mo couple. Error bars represent 3 standard deviations of the k-ratio mean measurements

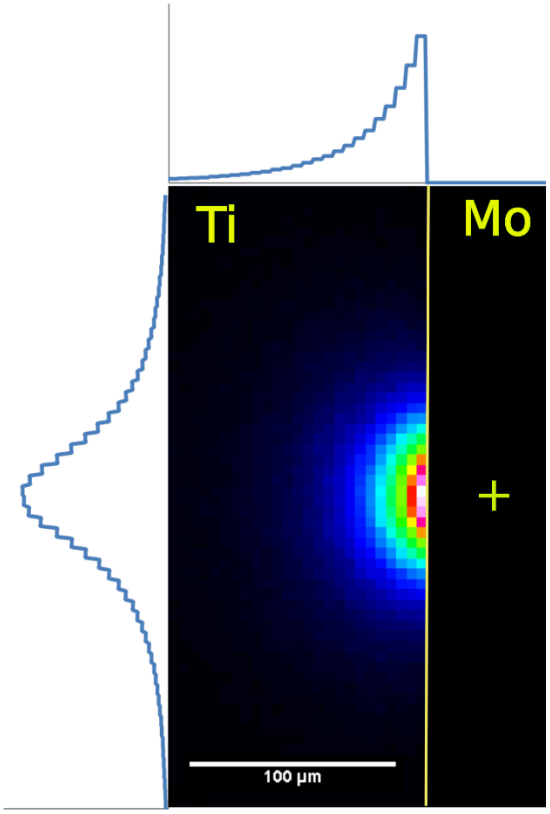

Figure 9. Simulated distribution of secondary fluorescent Ti Ka x-rays calculated using PENEPMA, i.e. the source of secondary fluorescent Ti K⟨ x-rays for an analysis made in Mo at 25µm away from the Mo/Ti interface. Displayed above and to the left are integrated intensity histograms. Of note is that the x-rays do not originate from a single point on the interface, but are distributed both along the interface and into the Ti.